The Astrophysical Journal, 982:91 (6pp), 2025 April 1 https://doi.org/10.3847/1538-4357/adb7e4
© 2025. The Author(s). Published by the American Astronomical Society.
OPEN ACCESS

A New Reaction Rate of the ^{27}Al(p,γ)^{28}Si Reaction Based on Indirect Low-energy Cross-section Measurements

M. La Cognata[1], S. Palmerini[2,3,4], F. Dell'Agli[4], P. Ventura[4], P. Adsley[5,6], R. Alba[1], S. Cherubini[1,7], M. Costa[1], A. Di Pietro[1], P. Figuera[1], G. L. Guardo[1], M. Gulino[1,8], F. Hammache[9], M. La Commara[10,11], L. Lamia[1,7,12], D. Lattuada[1,8], C. Maiolino[1], M. Mazzocco[13,14], A. Oliva[1], R. G. Pizzone[1,7], P. M. Prajapati[1], G. G. Rapisarda[1,7], S. Romano[1,7,12], D. Santonocito[1], M. L. Sergi[1,7], R. Spartá[1,8], and A. Tumino[1,8]

[1] Istituto Nazionale di Fisica Nucleare, Laboratori Nazionali del Sud, 95123 Catania, Italy; lacognata@lns.infn.it
[2] Dipartimento di Fisica e Geologia, Universitá degli Studi di Perugia, 06123 Perugia, Italy
[3] Istituto Nazionale di Fisica Nucleare, Sezione di Perugia, 06123 Perugia, Italy
[4] INAF, Observatory of Rome, 00077 Monte Porzio Catone (RM), Italy
[5] Cyclotron Institute, Texas A&M University, College Station, Texas 77843-3366, USA
[6] Department of Physics and Astronomy, Texas A&M University, College Station, Texas 77843-4242, USA
[7] Dipartimento di Fisica e Astronomia "Ettore Majorana," Università degli Studi di Catania, Catania 95123, Italy
[8] Dipartimento di Ingegneria e Architettura, Università degli Studi "Kore," 94100 Enna, Italy
[9] Université Paris-Saclay, CNRS/IN2P3, IJCLab, 91405 Orsay, France
[10] Dipartimento di Farmacia, Università di Napoli "Federico II," 80131 Napoli, Italy
[11] Istituto Nazionale di Fisica Nucleare, Sezione di Napoli, 80126 Napoli, Italy
[12] Centro Siciliano di Fisica Nucleare e Struttura della Materia, CSFNSM, 95123 Catania, Italy
[13] Dipartimento di Fisica e Astronomia, Università di Padova, 35131 Padova, Italy
[14] Istituto Nazionale di Fisica Nucleare, Sezione di Padova, Padova, Italy
Received 2024 November 21; revised 2025 February 11; accepted 2025 February 17; published 2025 March 21

Abstract

The Mg–Al cycle is characteristic of the high-temperature ($T \sim 0.055$ GK) H-burning of evolved stars and their nucleosynthesis. A proper comprehension of this reaction network can help in solving debated questions such as the occurrence of anticorrelation in Mg–Al abundances in globular clusters. Recent high-resolution surveys have shown that such an anticorrelation may hide the existence of multiple stellar populations and that the relative abundances of Mg isotopes may not be correlated with Al. Proton-induced reactions on ^{27}Al play a key role in this respect, in particular the interplay between the (p, α) and (p, γ) channels, determining the closure (or not) of the Mg–Al cycle. Presently, the situation is still debated owing to the large uncertainty affecting existing experimental nuclear data. A recent indirect measurement indicates a further reduction in the ^{27}Al(p, α)^{24}Mg reaction rate with respect to the ones commonly adopted in astrophysical models. In the present work, we update the ^{27}Al(p,γ)^{28}Si reaction rate based on the same indirect measurement results. In the case of AGB stars experiencing hot bottom burning, the revised rate would lead to a ∼35% increase in ^{27}Al abundance with respect to what is presently foreseen, with interesting astrophysical consequences.

Unified Astronomy Thesaurus concepts: Nuclear astrophysics (1129); Globular star clusters (656); Isotopic abundances (867)

1. Astrophysical Motivations

The Mg–Al cycle is not as relevant as the CNO cycle for energy production in stars because of the higher Coulomb barriers involved, yet it significantly influences the nucleosynthesis of Mg and Al isotopes due to the high-temperature ($T \sim 0.055$ GK) H-burning (C. Iliadis 2015). The closure of the Mg–Al cycle is still debated because of the uncertainties of the cross sections of the competing ^{27}Al(p, α)^{24}Mg and ^{27}Al(p, γ)^{28}Si reactions. In the temperature range 0.015–0.08 GK, uncertainties are so large that the dominant channel cannot be established, making astrophysical predictions unreliable (C. Iliadis 2015). This has called for a careful assessment of the ^{27}Al proton destruction cross sections in the energy range typical of stellar nucleosynthesis (around 100 keV). In the last years, indirect measurements have been carried out with the aim to better estimate the contribution of the ^{27}Al(p,α)^{24}Mg reaction rate (S. Palmerini et al. 2021; M. La Cognata et al. 2022a, 2022b). The measured cross section tends to disfavor the closure of the Mg–Al cycle in comparison with what could be expected from C. Iliadis et al. (2010a), yet uncertainties are still large.

Mg and Al abundances prove crucial in many astrophysical contexts. In particular, the Mg–Al anticorrelation observed in many globular clusters (GCs, e.g., NGC 2808, M4, M79) provides an important constraint on the phenomenon of multiple populations. While the occurrence of this anticorrelation is well established, the dependence on the cluster's mass and age is still a matter of debate (see, e.g., E. Pancino et al. 2017; I. Baeza et al. 2022; D. A. Alvarez Garay et al. 2024). The importance of the Mg–Al anticorrelation lies in the fact that, although it is generated by H-burning processes, the abundance variability of these two elements among stars of the same cluster is much broader than the spread observed in the CNO abundances. Since proton captures in the Mg–Al region occur at high temperatures (∼0.1 GK), the observation of these elements strongly constrains the type of star responsible for the Al enhancement in the cluster. The existence of multiple stellar populations and the lack of apparent correlation of the relative

Original content from this work may be used under the terms of the Creative Commons Attribution 4.0 licence. Any further distribution of this work must maintain attribution to the author(s) and the title of the work, journal citation and DOI.

abundances of ^{24}Mg, ^{25}Mg, and ^{26}Mg with Al (G. S. Da Costa et al. 2013; K. Lind et al. 2015) in the clusters suggest multiple polluters, including supermassive stars, massive binaries, massive fast-rotating stars, and intermediate-mass asymptotic giant branch (AGB) stars (E. Carretta & A. Bragaglia 2024, and references therein).

The stronger Mg–Al anticorrelation observed in GCs with lower metallicity would hint to the closure of the Mg–Al cycle at higher temperatures. However, the Al–Si correlation has also been observed in some clusters (e.g., ω–*Cen*, NGC 2298, NGC 6752, NGC 28008, M92, and M15; S. Mészáros et al. 2020; I. Baeza et al. 2022; D. A. Alvarez Garay et al. 2024), and this would indicate that the reaction network is instead open. Furthermore, S. Mészáros et al. (2020) suggest that the absence of correlation or the observation of a weak correlation of the Mg–Al–Si abundances in metal-rich clusters cannot be considered as evidence of the closure of the cycle because the estimate of the Al abundance may be affected by distortion effects due to high metallicity.

In this scenario, it is clear that to resolve the issue, an increase in sensitivity in stellar spectroscopy is crucial, as well as new, higher-precision measurements of the cross sections of the nuclear reactions involved in Mg–Al–Si nucleosynthesis. In particular, the branching between the ^{27}Al(p,α)^{24}Mg and ^{27}Al(p,γ)^{28}Si reactions is pivotal to determine whether and at what temperature the Mg–Al cycle is closed and, consequently, what the masses and nature of the polluters in clusters showing multiple stellar populations are.

Analyses carried out using the M. La Cognata et al. (2022a, 2022b) ^{27}Al(p,α)^{24}Mg reaction rate have shown that, in 4–8 $M_\odot$ stars experiencing hot bottom burning (HBB) during their AGB phase, limited changes are introduced in Mg–Al isotopic abundances with respect to what was deduced using the C. Iliadis et al. (2010a) reaction rate commonly adopted in stellar models. In detail, variations are small for metal-poor stars and stars with $M \gtrsim 5M_\odot$ and solar metallicity. In the case of a 4.5 $M_\odot$ solar-metallicity AGB, a ∼5% increase in the surface abundance of ^{27}Al is found, a difference that rises to ∼25% when the lower limits of the ^{27}Al(p,α)^{24}Mg reaction rates are used in calculations. Still, other isotopic abundances are scarcely affected (M. La Cognata et al. 2022a, 2022b).

The conclusions of M. La Cognata et al. (2022a, 2022b) resulted in the need for further investigation of the γ-ray channel, given the greater impact on elemental yields from intermediate-mass stars, in particular of ^{27}Al. For example, this is crucial in studying the multiple populations in GCs, where the winds of AGBs could act as pollutants of the interstellar medium from which new generations of stars have formed. Moreover, a better knowledge of the ^{27}Al(p, γ)^{28}Si may impact the understanding of ^{26}Al nucleosynthesis in the Galaxy and in the early solar system, with possible cosmo-chronological implications (D. Vescovi et al. 2018; A. M. Laird et al. 2023).

For these reasons, starting from the experimental data reported in M. La Cognata et al. (2022a, 2022b), in this work we supply a revised ^{27}Al(p,γ)^{28}Si reaction rate and evaluate some astrophysical consequences. For the first time, the reaction rate will be based on experimental data taken at the energies of astrophysical interest.

2. Status of the Art

Today's commonly accepted reaction rate for the ^{27}Al(p, γ)^{28}Si reaction is discussed at length in C. Iliadis et al. (2001, 2010a, 2010b). Focusing on the temperatures of interest, the total reaction rate has a ∼20% uncertainty above about 0.1 GK. The uncertainty amounts to about 1 order of magnitude below about 0.1 GK. Only at temperatures $\lesssim$0.015 GK is the direct capture contribution important. Therefore, we conclude that relevant studies must focus on resonant states around ∼100 keV above the proton emission threshold in ^{28}Si. Such an energy interval is critical since resonances were directly measured for $E_{\rm cm} \geqslant 195$ keV[15] (C. Iliadis et al. 2001). The impact of the resonances can be estimated by comparing the older C. Angulo et al. (1999) rate with the C. Iliadis et al. (2001) one, where the improved determination of spectroscopic factors for the near-threshold states leads to reaction-rate changes of up to a factor of 20 in the reaction rate below ∼0.07 GK.

The ^{27}Al(p, γ)^{28}Si reaction rate at low temperatures is determined by the properties of the 71.5 keV and 84.3 keV resonances, whose strengths are evaluated starting from the reanalysis of the ^{27}Al(^{3}He,d)^{28}Si stripping data of A. E. Champagne et al. (1986). For both of them, only upper limits are available. For $E_{\rm cm} = 71.5$ keV the measured deuteron angular distribution indicated a dominant $l = 2$ contribution though a small $l = 0$ contribution could not be excluded. For $E_{\rm cm} = 84.3$ keV, the measured deuteron angular distribution could be fitted adopting $l = 1$ or $l = 3$ contributions and the upper limit was set assuming a pure $l = 1$ transfer (C. Iliadis et al. 2001). Slightly above the energy range of astrophysical interest, we stress the occurrence of an unresolved triplet of resonances at $E_{\rm cm} = 193.4$ keV, 193.5 keV, and 195.5 keV, for which the overall strength is attributed to the latter in calculations (C. Iliadis et al. 2010a).

3. The THM Resonance Strengths

Recently, the ^{27}Al(p,α)^{24}Mg reaction was indirectly studied (S. Palmerini et al. 2021; M. La Cognata et al. 2022a, 2022b) using the Trojan Horse Method (THM; see A. Tumino et al. 2021 for a recent review, and M. La Cognata et al. 2010; R. E. Tribble et al. 2014 for details on the data analysis method and the theoretical formalism, respectively). Thanks to the THM approach, it was possible to firmly establish the strength of the 84.3 keV resonance in the ^{27}Al(p,α)^{24}Mg reaction and set a factor of ∼3 lower upper limit on the 71.5 keV resonance strength. Other resonances were observed, and measurements of resonance strengths or tighter upper limits of those strengths were set for resonances up to about 1400 keV (see Table 2 of M. La Cognata et al. 2022b for details). Thanks to the possibility to fully span the energy region of astrophysical interest, in this work we will use the same data as in M. La Cognata et al. (2022b) to obtain new measurement-based ^{27}Al(p, γ)^{28}Si resonance strengths, with particular emphasis on the $E_{\rm cm} = 71.5$ keV and 84.3 keV resonances.

The 71.5-keV resonance. From C. Iliadis et al. (2010a) we know that $\Gamma_p << \Gamma_\gamma << \Gamma_\alpha$.[16] This chain of inequalities leads to a resonance strength $\omega\gamma$ of the (p, α) channel that is directly proportional to Γ_p through the statistical factor ω. This is what we expect at deeply sub-Coulomb energies where the p–channel is suppressed by the Coulomb barrier. Focusing on the (p, γ) channel instead, the previous equations result in a resonance strength proportional to $\Gamma_p\Gamma_\gamma/\Gamma_\alpha$. Since the THM measurement (M. La Cognata et al. 2022b) could set a more

[15] Where $E_{\rm cm}$ is the energy in the framework of the center of mass of the colliding nuclei.

[16] Where Γ is the total width of resonance and Γ_i is the partial width for emission of the particle i.

Table 1
List of Updated Resonance Strengths or Upper Limits for the ^{27}Al(p, γ)^{28}Si Reaction, Based on the THM Results (M. La Cognata et al. 2022a, 2022b)

E_i^R (keV) (1)	$\omega\gamma$ (C. Iliadis et al. 2010a) (eV) (2)	$\omega\gamma$ (present work) (eV) (3)	$\omega\gamma$ (p, α) (eV) (4)
71.5	$\leqslant 6 \times 10^{-15}$	$\leqslant 2 \times 10^{-15}$	$\leqslant 8.23 \times 10^{-15}$
84.3	$\leqslant 4 \times 10^{-13}$	$2.5 \pm 1.3 \times 10^{-14}$	$1.67 \pm 0.32 \times 10^{-14}$
705.08	0.129 ± 0.007	0.077 ± 0.004	0.261 ± 0.065

Note. Resonance energies, strengths from C. Iliadis et al. (2010a), and revised values from this work are listed in columns (1), (2), and (3), respectively. In column (4), the strengths of the (p, α) channel from Table 2 of M. La Cognata et al. (2022b) are given for reference.

stringent upper limit on the (p, α) channel resonance strength, this implies a tighter limit on Γ_p that translates on a correspondingly lower upper limit on the (p, γ) channel resonance strength. From Table 2 of M. La Cognata et al. (2022b; see also column (4) of Table 1) we calculate the scaling factor to equal 33%, leading to a new recommended (p, γ) resonance strength upper limit equal to 2×10^{-15} eV.

The 84.3-keV resonance. The situation for such resonance is different from the one at 71.5 keV, since the p-width is much smaller than the α and γ partial widths, which are similar (C. Iliadis et al. 2010a). From $\Gamma_p << \Gamma_\gamma \sim \Gamma_\alpha$, we deduce that the ($p$, α) channel resonance strength is still proportional to Γ_p through the $\Gamma_\alpha/(\Gamma_\gamma + \Gamma_\alpha) \sim 0.5$ factor, similarly to the (p, γ) strength also proportional to Γ_p through the $\Gamma_\gamma/(\Gamma_\gamma + \Gamma_\alpha) \sim 0.5$ factor. Using the definition of resonance strength, we can calculate Γ_p from Table 2 of M. La Cognata et al. (2022b; column (4) of Table 1), $\Gamma_p = 1.67 \pm 0.59 \times 10^{-13}$ eV. We emphasize that this is not an upper limit since in M. La Cognata et al. (2022a, 2022b) we determine the resonance strength. Using the THM Γ_p, we can calculate the strength for the (p, γ) channel, which is $2.5 \pm 1.3 \times 10^{-14}$ eV. The increase in the uncertainty with respect to the THM measurement is due to the fact that Γ_γ and Γ_α from C. Iliadis et al. (2010a) are used in the calculation.

The triplet around 200 keV. The situation for the triplet at $E_{\rm cm} = 193.4$ keV, 193.5 keV, and 195.5 keV resonance energies is complicated by the fact that such states are not resolved. In M. La Cognata et al. (2022b), following the discussion in C. Iliadis et al. (2010a), the 193.5 keV resonance (corresponding to the ^{28}Si level at 11.779 MeV) was assumed to dominate the overall contribution. However, such a recommendation is not proposed for the (p, γ) channel, for which the whole strength was attributed to the 195.5 keV resonance. Therefore, for such a group of resonances, the strengths in the literature will be considered.

The 214.7 keV resonance. Since the THM measurement could only set an upper limit on the 214.7 keV resonance strength, we consider that the 214.7 keV resonance from C. Iliadis et al. (2010a) has a better accuracy than the one we could estimate from our upper limit, so we do not provide a new THM-based estimate of the 214.7 keV resonance strength.

The 486.74 keV resonance. Based on the THM measurement, we cannot recommend any updated strength for this resonance given the relation between the partial widths: $\Gamma_\gamma << \Gamma_p < \Gamma_\alpha$. While the ($p$, γ) resonance strength is proportional to Γ_γ, the (p, α) channel resonance strength is proportional to $\Gamma_p\Gamma_\alpha/(\Gamma_p + \Gamma_\alpha)$, so we cannot introduce any updated constraint on the former since we are not sensitive to Γ_γ.

Resonance from 609.49 keV to 903.54 keV. For these resonances, strengths are available in C. Iliadis et al. (2010a), with no details on the partial widths. From the inspection of Table 2 of M. La Cognata et al. (2022b; column (4) of Table 1), it is apparent that the strengths we deduced from the THM measurement are in good agreement with those in our reference work, except for the 705.08 keV resonance. Leaving the latter aside, the THM data therefore confirm the strength values for the (p, γ) channel listed in C. Iliadis et al. (2010a). In the case of the 705.08 keV resonance, our analysis shows that the main source of difference is the different spin-parity assignment (see M. La Cognata et al. 2022b for more details). This leads to a revised resonance strength of 0.077 ± 0.004 eV.

The resonances at 1140.88 keV, 1316.7 keV, and 1388.8 keV. In the case of the 1140.88 keV and 1316.7 keV resonances, the analysis of the partial widths entail that our revised (p, α) resonance strengths cannot be used to draw conclusions on the (p, γ) ones. In the case of the 1388.8 keV resonance, the deduced scaling factor agrees with the unit, so the THM results do not suggest any revision of the recommended strength listed in C. Iliadis et al. (2010a).

The updated resonance strengths are listed in Table 1.

4. The New Reaction Rate Based on THM Data

For astrophysical applications, we calculated the reaction rate by adopting the detailed Monte Carlo method that makes use of the code `RatesMC` (C. Iliadis et al. 2010a, 2015). The main advantage of the code is a statistically sound treatment of the uncertainties, including the use of the Porter-Thomas distribution to properly account for upper limits on the resonance strengths, as well as of lognormal probability density for measured resonance strengths and for the reaction rate. In particular, we will express the low rate, median (best) rate, and high rate as the 16th, 50th, and 84th percentiles of the cumulative rate distribution, respectively, as discussed, e.g., in A. L. Sallaska et al. (2013).

In the calculation of the updated reaction rate we adopted the resonance strengths listed in Table 1. All other parameters were taken from C. Iliadis et al. (2010a). As a consequence, significant deviations from the STARLIB rate are present only in a limited temperature region ~0.02–0.08 GK (Figure 1) that, indeed, is the one of greatest astrophysical interest. In Figure 1, the green line is the ratio of the STARLIB rate (C. Iliadis et al. 2010b) to the THM one, and it shows a reduction in the reaction rate by a factor of 3 with respect to the one mostly used in astrophysical models. The contour plot in the same figure, displaying the rate probability density, is used to highlight the overall error budget affecting the THM updated reaction rate. The thick lines are used to encompass the 68% confidence interval, while the thin lines are used for the 95% one.

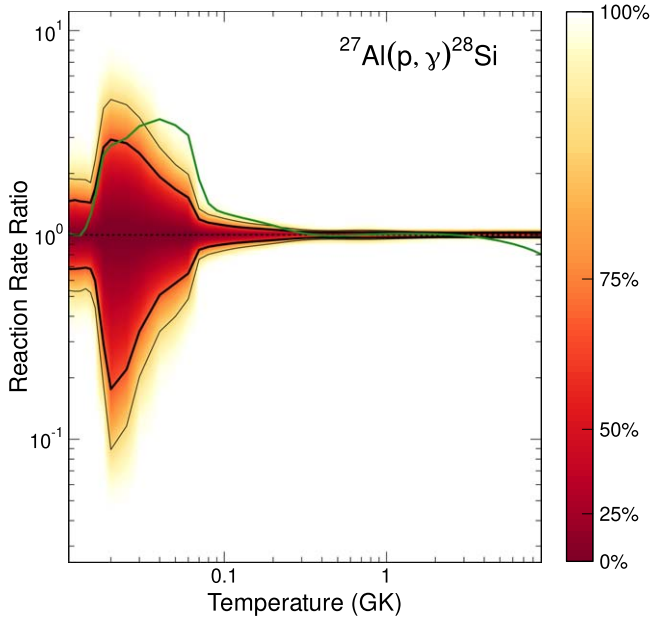

Figure 1. Green line: ratio of the STARLIB median reaction rate (C. Iliadis et al. 2010b) to the one calculated with the same statistical approach, using the THM updated resonance strengths in Table 1. A significant reduction in the median rate is apparent. The contour plot shows the uncertainty of the THM reaction rate, taken equal to one over the whole examined temperature range. The thick lines are used to encompass the 68% confidence interval, while the thin lines are used for the 95% one.

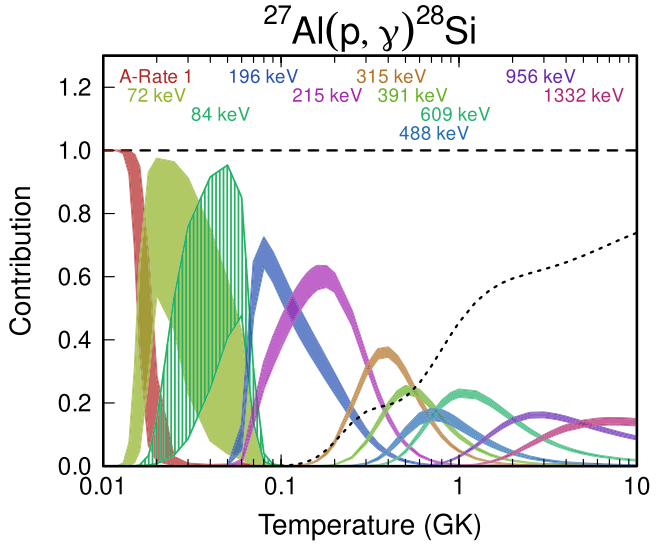

Figure 2. Fractional contributions of the most relevant resonances in the ^{27}Al(p,γ)^{28}Si astrophysical factor to the total reaction rate. The present work's strengths are used when available, as listed in Table 1, otherwise the same contributions as in C. Iliadis et al. (2010a) are considered. Hatched areas encompass the $\pm 1\sigma$ uncertainty range, while a dotted line is used for the contribution of higher energy resonances. "A-Rate 1" refers to the nonresonant (direct capture) rate contribution.

Figure 2 makes it possible to better understand the main sources of uncertainties since the figure displays the fractional contribution of each resonance to the reaction rate. In detail, since we could observe the 84.3 keV resonance in the present work, we can effectively constrain the reaction rate at temperatures ∼0.07–0.08 GK, which are the temperatures of primary astrophysical interest; at lower temperatures, uncertainties grow larger owing to the fact we could only set upper limits for the strengths of the states at 71.5 keV. For higher temperatures, the result coincides essentially with the STARLIB reaction rate (C. Iliadis et al. 2010a).

5. The Impact on Astrophysics

The significant reduction in the ^{27}Al(p,γ)^{28}Si reaction rate below ∼0.1 GK might have important consequences on the understanding of nucleosynthesis involving the Mg–Al cycles and the relative abundances of Mg and Al isotopes.

We have investigated the nucleosynthesis of an AGB star with the mass and the metallicity it should have, in the case that it were a plausible polluter in Al of GCs, namely, 6 $M_{\odot}$ and $Z = 6 \times 10^{-4}$ (P. Ventura et al. 2016). This mass is among those that activate HBB, and the temperatures reached at the bottom of the convective envelope are high enough to allow one to appreciate substantial differences in the chemical yields between the stellar models calculated with different reaction rates for the ^{27}Al(p,γ)^{28}Si reaction.

The stellar models have been computed using the ATON code for stellar evolution. The numerical structure is detailed in P. Ventura et al. (1998), while an exhaustive description of the updated version that models the AGB phase can be found in P. Ventura & F. D'Antona (2005a, 2005b). The ATON code allows us to track the full evolution of low- and intermediate-mass stars, from the pre-main sequence to the white dwarf cooling phase. Nuclear burning and chemical mixing are self-consistently coupled using a diffusive scheme, where convective velocities decay exponentially with distance from the boundary. The temperature gradient in convectively unstable regions is determined through the full spectrum turbulence model (V. M. Canuto & I. Mazzitelli 1991). The mass-loss prescription from T. Bloecker (1995) has been assumed for the AGB phase computations, where the η parameter regulates the efficiency of the mass-loss process. To consider the impact mass-loss rate on the AGB nucleosynthesis (P. Ventura & F. D'Antona 2005b), we explored two cases: $\eta = 0.02$ (solid curves in Figure 3), found to reproduce the relative number of luminous lithium-rich AGBs in the Magellanic Clouds with respect to the number of luminous AGB stars (P. Ventura et al. 2000) and $\eta = 0.002$, which protracts the duration of the AGB evolution by a factor of 3.

In Figure 3 we compare the evolutions of the abundances of ^{24}Mg, ^{27}Al, and ^{28}Si (namely, the most abundant isotopes of their element) in the stellar envelope calculated with the rates of C. Iliadis et al. (2010b; black) and the one calculated in the previous section (red). The ^{27}Al(p,α)^{24}Mg reaction rate by M. La Cognata et al. (2022a, 2022b) has also been employed in the latter. Substantial differences can be observed: the updated THM-based reaction rate allows the accumulation of much more ^{27}Al; at the peak of production, we find about 35% more than in the case of C. Iliadis et al. (2010b). The final abundance of ^{28}Si is affected too, with a reduction of 15%, while variations in the content of ^{24}Mg are negligible. The sensitivity to the nuclear inputs used is preserved for both the mass-loss rates assumed.

By observing the evolution of the abundances in Figure 3, both the Mg–Al and the Mg–Si anticorrelation and the Al–Si correlation can be easily inferred. Such findings provide further support for the hypothesis that AGBs are responsible for the trends observed in clusters with multiple populations. In the bottom-right panel of Figure 3, the correlation between ^{27}Al and ^{28}Si is less pronounced when the ^{27}Al(p, γ)^{28}Si reaction rate from this work is adopted and a higher mass-loss rate is considered. This difference becomes negligible when the lower

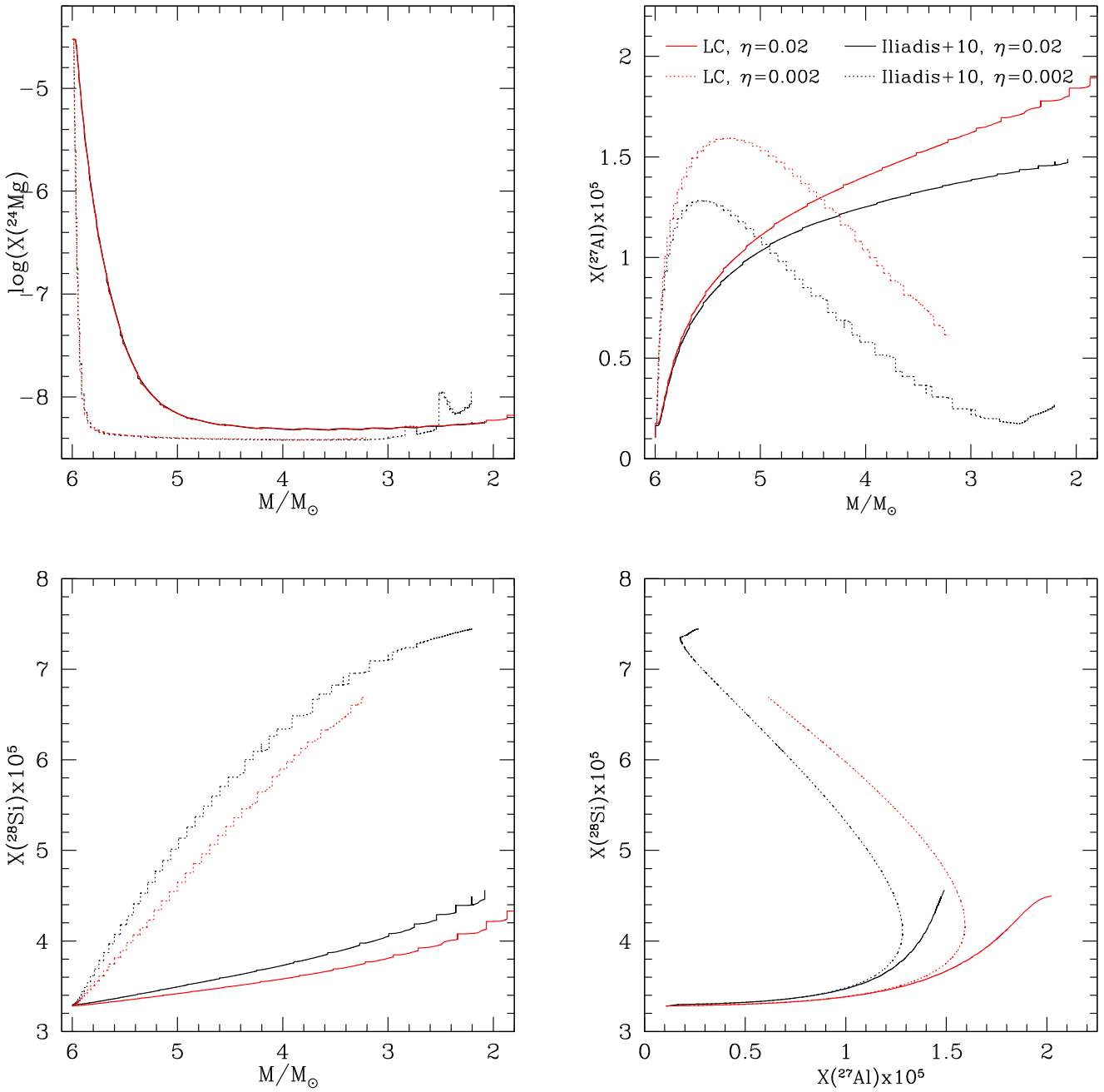

Figure 3. Surface abundance of ^{24}Mg (top-left panel), ^{27}Al (top-right panel), and ^{28}Si (bottom-left panel) as a function of the mass of the star during the AGB evolution of a 6 $M_{\odot}$ star with metallicity $Z = 6 \times 10^{-4}$. The ^{27}Al vs. ^{28}Si relation is shown in the bottom-right panel. The comparison is among the C. Iliadis et al. (2010b) rate (black) and the present work's rate (red). Both evolutions are calculated with a standard mass-loss prescription (solid line) and for a lower mass-loss rate (dotted line) by the ATON stellar evolutionary code (P. Ventura et al. 2008).

mass-loss rate is used, as the longer AGB evolution allows for the destruction of aluminum. This fact does not invalidate our conclusions, but it would hint to a variation in the branching of the exit channels of the ^{27}Al+p reaction in favor of the (p,α) channel and thus of the closure of the Mg–Al cycle (at least in the temperature range at which it is burnt in our case of study).

Acknowledgments

The authors are grateful to the LNS director and to the technical staff who made it possible to carry out a successful experiment under safe conditions, given the ongoing pandemic, right after Spring 2020 lockdown, thus restarting LNS accelerator-driven research activity.

Software: RatesMC, ATON.

ORCID iDs

M. La Cognata https://orcid.org/0000-0002-1819-4814
S. Palmerini https://orcid.org/0000-0001-5386-8389
P. Ventura https://orcid.org/0000-0002-5026-6400
L. Lamia https://orcid.org/0000-0002-4055-0811

References

Alvarez Garay, D. A., Mucciarelli, A., Bellazzini, M., Lardo, C., & Ventura, P. 2024, A&A, 681, A54
Angulo, C., Arnould, M., Rayet, M., et al. 1999, NuPhA, 656, 3
Baeza, I., Fernández-Trincado, J. G., Villanova, S., et al. 2022, A&A, 662, A47

Bloecker, T. 1995, A&A, 297, 727
Canuto, V. M., & Mazzitelli, I. 1991, ApJ, 370, 295
Carretta, E., & Bragaglia, A. 2024, A&A, 690, A158
Champagne, A. E., Pitt, M. L., Zhang, P. H., Lee, L. L., & Levine, M. J. 1986, NuPhA, 459, 239
Da Costa, G. S., Norris, J. E., & Yong, D. 2013, ApJ, 769, 8
Iliadis, C. 2015, Nuclear Physics of Stars (New York: Wiley)
Iliadis, C., D'Auria, J. M., Starrfield, S., Thompson, W. J., & Wiescher, M. 2001, ApJS, 134, 151
Iliadis, C., Longland, R., Champagne, A. E., & Coc, A. 2010a, NuPhA, 841, 251
Iliadis, C., Longland, R., Champagne, A. E., Coc, A., & Fitzgerald, R. 2010b, NuPhA, 841, 31
Iliadis, C., Longland, R., Coc, A., Timmes, F. X., & Champagne, A. E. 2015, JPhG, 42, 034007
La Cognata, M., Palmerini, S., Adsley, P., et al. 2022a, PhLB, 826, 136917
La Cognata, M., Palmerini, S., Adsley, P., et al. 2022b, ApJ, 941, 96
La Cognata, M., Spitaleri, C., Mukhamedzhanov, A., et al. 2010, ApJ, 708, 796
Laird, A. M., Lugaro, M., Kankainen, A., et al. 2023, JPhG, 50, 033002
Lind, K., Koposov, S. E., Battistini, C., et al. 2015, A&A, 575, L12
Mészáros, S., Masseron, T., Garcìa-Hernández, D. A., et al. 2020, MNRAS, 492, 1641
Palmerini, S., La Cognata, M., Hammache, F., et al. 2021, EPJP, 136, 898
Pancino, E., Romano, D., Tang, B., et al. 2017, A&A, 601, A112
Sallaska, A. L., Iliadis, C., Champange, A. E., et al. 2013, ApJS, 207, 18
Tribble, R. E., Bertulani, C. A., Cognata, M. L., Mukhamedzhanov, A. M., & Spitaleri, C. 2014, RPPh, 77, 106901
Tumino, A., Bertulani, C. A., La Cognata, M., et al. 2021, ARNPS, 71, 345
Ventura, P., & D'Antona, F. 2005a, A&A, 431, 279
Ventura, P., & D'Antona, F. 2005b, A&A, 439, 1075
Ventura, P., D'Antona, F., & Mazzitelli, I. 2000, A&A, 363, 605
Ventura, P., D'Antona, F., & Mazzitelli, I. 2008, Ap&SS, 316, 93
Ventura, P., Zeppieri, A., Mazzitelli, I., & D'Antona, F. 1998, A&A, 334, 953
Ventura, P., Garcìa-Hernández, D. A., Dell'Agli, F., et al. 2016, ApJL, 831, L17
Vescovi, D., Busso, M., Palmerini, S., et al. 2018, ApJ, 863, 115